

Electron and muon $g - 2$, radiative neutrino mass, and $\ell' \rightarrow \ell\gamma$ in a $U(1)_{e-\mu}$ model

Chuan-Hung Chen^{1,*} and Takaaki Nomura^{2,†}

¹*Department of Physics, National Cheng-Kung University, Tainan 70101, Taiwan*

²*School of Physics, KIAS, Seoul 02455, Korea*

(Dated: April 6, 2022)

Abstract

A nonconventional $U(1)_{e-\mu}$ gauge model is proposed to explain the unexpected anomalous magnetic moments of the electron and muon (lepton $g - 2$), where only the right-handed electron and muon in the standard model carry the $U(1)_{e-\mu}$ charge. Although the light lepton masses are suppressed when the gauge symmetry is spontaneously broken, they can be generated through the Yukawa couplings to newly introduced particles, such as vector-like lepton doublets and singlets, and scalar singlets. It is found that the same Yukawa couplings combined with the new scalar couplings to the Higgs can induce the radiative lepton-flavor violation processes $\ell' \rightarrow \ell\gamma$ and lepton $g - 2$, where the lepton $g - 2$ is proportional to m_ℓ . When Majorana fermions and a scalar singlet are further added into the model, the active neutrinos can obtain masses via the radiative seesaw mechanism. When the bounds from the m_e and m_μ and the neutrino data are satisfied, we find that the electron $g - 2$ can reach an order of -10^{-12} , and the muon $g - 2$ can be an order of 10^{-9} . In addition, when the $\mu \rightarrow e\gamma$ decay is suppressed, the resulting branching ratio for $\tau \rightarrow e\gamma$ can be of $O(10^{-8})$, and that for $\tau \rightarrow \mu\gamma$ can be as large as the current upper limit.

*Electronic address: physchen@mail.ncku.edu.tw

†Electronic address: nomura@kias.re.kr

I. INTRODUCTION

A potential hint for new physics has been found in the muon anomalous magnetic moment (muon $g - 2$) since the E821 experiment at Brookhaven National Lab (BNL) [1] reported a 3.3σ deviation from the standard model (SM) prediction, which is shown as [2, 3]:

$$\delta a_\mu = a_\mu^{\text{exp}} - a_\mu^{\text{SM}} = (26.1 \pm 7.9) \times 10^{-10}. \quad (1)$$

A 3.7σ deviation was also obtained by the lattice calculations as $\delta a_\mu = (27.4 \pm 7.3) \times 10^{-10}$ [4] and $\delta a_\mu = (27.06 \pm 7.26) \times 10^{-10}$ [5]. Due to the discrepancy between the experimental measurement and the theoretical prediction, various solutions have been proposed to resolve the anomaly over the years [6–32]. Although the recent result on the hadron vacuum polarization (HVP), which was calculated by Budapest- Marseille-Wuppertal (BMW) collaboration [33], weakens the necessity of a new physics effect, it is shown in [34] that the BMW result leads to new tensions with the HVP extracted from e^+e^- data and the global fits to the electroweak precision observables.

The new muon $g - 2$ measurements performed in the E989 experiment at Fermilab and the E34 experiment at J-PARC aim for a precision of 0.14 ppm [35] and 0.10 ppm [36], in which the experimental accuracy can be improved by a factor of 4 and 5, respectively. If we assume the future experimental and theoretical uncertainties can be respectively reduced by a factor of 4 and $\sqrt{2}$, it is expected that with a 3σ measurement, $\delta a_\mu \approx (12 \pm 4) \times 10^{-10}$ can be observed by the Fermilab muon $g - 2$ experiment [35].

Applying the most accurate measurement of the fine structure constant, which is measured using ^{133}Cs , to the theoretical calculations [37, 38], it is found that the difference in the electron $g - 2$ between the experiment and the SM result has a 2.4σ deviation and is expressed as [39]:

$$\delta a_e = -(8.8 \pm 3.6) \times 10^{-13}. \quad (2)$$

Differing from the muon $g - 2$, the electron $g - 2$ experimental value is lower than the SM result. In order to simultaneously explain the anomalistic electron and muon $g - 2$, some possible resolutions are provided in studies in the literature [40–58].

Inspired by the lepton $g - 2$ anomalies, we investigate an anomaly-free gauged $U(1)_{e-\mu}$ extension of the SM. For a light Z' gauge boson, the potential strict constraints are from the $\nu - e$ scattering [59] and the neutrino trident production experiments [60, 61]. In

order to escape from the neutrino-related experimental constraints, unlike the conventional $U(1)_{e-\mu}$, where the associated Z' -gauge boson simultaneously couples to the right-handed lepton singlets and the left-handed lepton doublets in the SM [62], we propose that the $U(1)_{e-\mu}$ only couples to the right-handed leptons.

The immediate problem with the $U(1)_{e-\mu}$ model is the massless electron and muon. To resolve this problem, we add new representations into the model, such as vector-like lepton doublets and singlets, and scalar singlets, where with the exception of one vector-like lepton singlet, they all carry the $U(1)_{e-\mu}$ charges. Thus, the lepton masses can be generated through the mixings with the introduced heavy charged leptons at the tree level.

It is found that when the new scalar couplings are considered, the same effects, which lead to the light lepton masses, can induce the radiative lepton-flavor violation (LFV) processes at the one-loop level. Taking the initial and final leptons to be the same species, the electron and muon $g-2$ can then be generated. Because the effect on the τ $g-2$ is small, we do not further discuss the influence on the τ -lepton. We note that since the Z' -gauge boson only couples to the right-handed light leptons, the induced lepton $g-2$ values are negative [63, 64], and the resulting ratio is $\delta a_e^{Z'}/\delta a_\mu^{Z'} \sim m_e^2/m_\mu^2$. If we use the Z' effect as the single source leading to the negative electron $g-2$, the resulting muon $g-2$ is also negative and contradicts the indications in the current data. Therefore, in this study, the $g_{Z'}$ gauge coupling and $m_{Z'}$ have to be taken in such a way that the induced muon $g-2$ is small enough. We will show that the observed lepton $g-2$ anomalies and the light lepton masses can be accommodated in the model.

We further find that when two Majorana fermions and one scalar singlet, which carry the $U(1)_{e-\mu}$ charge, are introduced, the neutrino mass can be radiatively produced through the one-loop Feynman diagrams. Since some of the involved parameters are related to parameters that contribute to $m_{e,\mu}$ and $\delta a_{e,\mu}$, it is found that when the bounds from the current neutrino data are satisfied, besides the fact that m_e and m_μ can fit the experimental values, the results of $\delta a_e \sim O(-10^{-12})$ and $\delta a_\mu \sim O(10^{-9})$ can be obtained.

When the rare $\mu \rightarrow e\gamma$ decay is suppressed in the study, and all the relevant constraints are satisfied, we find that in the model, the branching ratio (BR) for $\tau \rightarrow e\gamma$ can be under the current experimental upper bound. When we use constrained parameter values to estimate the BR for $\tau \rightarrow \mu\gamma$, it is found that $BR(\tau \rightarrow \mu\gamma)$ can be over the current upper limit; that is, the $\tau \rightarrow \mu\gamma$ decay can be used to further constrain the free parameter space. Nevertheless,

the results of $\delta a_e \sim O(-10^{-12})$ and $\delta a_\mu \sim O(10^{-9})$ are not influenced.

The paper is organized as follows: We introduce the model and discuss the relevant Yukawa couplings and the scalar potential in Sec. II. The vacuum stability conditions are also analyzed in this section. We discuss the tree-level charged lepton mass matrix and the loop-level neutrino mass matrix in Sec. III. In Sec. IV, we formulate the radiative LFV processes and lepton $g - 2$, and the numerical analysis is shown in Sec. V. We provide a summary in Sec. VI.

II. MODEL

In order to explain the neutrino data and the electron and muon $g - 2$, we consider an anomaly-free gauged $U(1)_{e-\mu}$ extension of the SM [62], where the associated Z' -gauge boson only couples to the right-handed electron and muon. We add new representations, such as two vector-like lepton doublets ($X^\ell, \ell = e, \mu$), one vector-like lepton singlets (X), two right-handed neutrino singlets (N^ℓ), three scalar singlets S^ℓ, S . In addition, for the $U(1)_{e-\mu}$ gauge anomaly cancellation, we need to introduce two vector-like lepton singlets (Σ^ℓ), where their masses arise from the new scalar singlet η . For these fields, we impose a Z_3 symmetry to suppress the interactions with the SM fermions. The representations and charge assignments of particles are given in Table I. The other SM particles, which are not shown in the table, do not have the $U(1)_{e-\mu}$ charges.

TABLE I: Representations and charge assignments of particles in $SU(2)_L \times U(1)_Y \times U(1)_{e-\mu} \times Z_3$ where $\omega^3 = 1$ with $\omega^* = \omega^2$.

| | e_R/μ_R | $X_{L,R}^{e/\mu}$ | $N^{e/\mu}$ | $S^{e/\mu}$ | S | $X_{L,R}$ | $\Sigma_{L(R)}^e$ | $\Sigma_{L(R)}^\mu$ | η |
|----------------|-------------|-------------------|-------------|-------------|-----|-----------|--------------------|---------------------|----------|
| $SU(2)_L$ | 1 | 2 | 1 | 1 | 1 | 1 | 1 | 1 | 1 |
| $U(1)_Y$ | -1 | -1/2 | 0 | 0 | 0 | -1 | -1 | -1 | 0 |
| $U(1)_{e-\mu}$ | $1/-1$ | $1/-1$ | $1/-1$ | $1/-1$ | 2 | 0 | $1(0)$ | $-1(0)$ | 1 |
| Z_3 | 0 | 0 | 0 | 0 | 0 | 0 | $\omega^2(\omega)$ | $\omega(\omega^2)$ | ω |

The gauge invariant Yukawa couplings for the lepton sector can be partly written as:

$$\begin{aligned}
-\mathcal{L}_Y = & \bar{L}_\tau y_\tau H \tau_R + \bar{X}_L y_\ell \ell_R S^{\ell\dagger} + \bar{L}_{\ell'} \tilde{y}_{\ell'} H X_R + \bar{L}_{\ell'} y_{\ell'}^\ell X_R^\ell S^{\ell\dagger} \\
& + \overline{X}_L^\ell y_X^\ell H \ell_R + \overline{X}_L^\ell \tilde{y}_X^\ell \tilde{H} N^\ell + h_e N^{eT} C N^e S + h_\mu N^{\mu T} C N^\mu S^\dagger \\
& + M_{X^\ell} \overline{X}_L^\ell X_R^\ell + M_X \bar{X}_L X_R + m_{N_{\mu e}} N^{eT} C N^\mu + H.c. ,
\end{aligned} \tag{3}$$

where $C = i\gamma^0\gamma^2$, and L and H are respectively the SM lepton and Higgs doublets; $\ell = e, \mu$, and ℓ' denotes all of the SM lepton-flavor indices. Since τ_R does not carry the $U(1)_{e-\mu}$ charge, after electroweak symmetry breaking (EWSB), the tau-lepton can obtain mass through the Higgs mechanism and its mass is expressed as $m_\tau^0 = y_\tau v/\sqrt{2}$, where v is the vacuum expectation value (VEV) of H . Although the electron and muon masses are suppressed in Eq. (3), we will show that their masses can be induced through the mixings with X^ℓ and X . The Yukawa couplings related to Σ^ℓ are expressed as:

$$\begin{aligned}
-\mathcal{L}_{\Sigma^\ell} = & y_\Sigma^e \bar{\Sigma}_L^e \Sigma_R^e \eta + y_\Sigma^\mu \bar{\Sigma}_L^\mu \Sigma_R^\mu \eta^\dagger + \overline{\Sigma}_L^e \Sigma_R^\mu (f_e S^e + f_\mu S^{\mu\dagger}) \\
& + \overline{\Sigma}_L^\mu \Sigma_R^e (g_e S^{e\dagger} + g_\mu S^\mu) + H.c.
\end{aligned} \tag{4}$$

In the model, the VEVs of S^ℓ will be taken to be around 1 GeV; thus, the Σ^ℓ masses are mainly dictated by the VEV of η and are formulated as $m_{\Sigma^\ell} \approx y_\Sigma^\ell v_\eta/\sqrt{2}$. Since the role of Σ^ℓ is used to cancel the $U(1)_{e-\mu}$ gauge anomaly, their effects are irrelevant to the study. Therefore, we will not further discuss the effects in Eq. (4) in the following analysis.

Since the electron and muon masses, the lepton $g-2$, and the neutrino masses are strongly correlated to the VEVs of scalar fields and the scalar couplings in the scalar potential, we have to discuss the vacuum stabilities of the scalar fields. We note that the singlet scalar η is introduced to obtain the Σ^ℓ masses. Although it can couple to other scalar fields, because these couplings do not significantly affect the phenomena, which we study; for simplicity, we take these couplings to be small. As a result, the scalar potential related to η can be approximated as:

$$V(\eta) \approx -\mu_\eta^2 \eta^\dagger \eta + \lambda_\eta (\eta^\dagger \eta)^2. \tag{5}$$

The VEV of η can be determined as $v_\eta = \sqrt{\mu_\eta^2/\lambda_\eta}$.

Based on the gauge symmetry, the scalar potential related to the scalar fields, such as H ,

S^ℓ , and S , are written as:

$$\begin{aligned}
V = & -\mu_H^2 H^\dagger H + \lambda_H (H^\dagger H)^2 + \mu_S^2 S^\dagger S + \lambda_S (S^\dagger S)^2 + \sum_{\ell=e,\mu} (\mu_{S^\ell}^2 S^{\ell\dagger} S^\ell + \lambda_{S^\ell} (S^{\ell\dagger} S^\ell)^2) \\
& + \lambda_{HS} H^\dagger H S^\dagger S + \sum_{\ell=e,\mu} \lambda_{HS^\ell} H^\dagger H S^{\ell\dagger} S^\ell + \lambda_{\mu e} (S^e S^{e\dagger}) (S^\mu S^{\mu\dagger}) \\
& + [\mu_{\mu e}^2 S^e S^\mu + \mu_{ee} (S^e)^2 S^\dagger + \mu_{\mu\mu} (S^\mu)^2 S + \tilde{\mu}_{\mu e} S^e S^{\mu\dagger} S^\dagger + \lambda_H^{\mu e} H^\dagger H S^e S^\mu \\
& + \lambda_S^{e\mu} S^e S^\mu S^\dagger S + \sum_{\ell=e,\mu} \lambda_{S^\ell}^{e\mu} S^e S^\mu S^{\ell\dagger} S^\ell + \lambda'_{\mu e} (S^e S^\mu)^2 + H.c.] \quad (6)
\end{aligned}$$

Using the neutral scalar fields, which are expanded around their VEVs and defined as:

$$H^0 = \frac{v + \phi}{\sqrt{2}}, \quad S = \frac{v_S + s}{\sqrt{2}}, \quad S^\ell = \frac{v_{S^\ell} + s^\ell}{\sqrt{2}}, \quad (7)$$

the minimal conditions of the VEVs can be found as:

$$\begin{aligned}
v^2 = & \frac{\mu_H^2}{\lambda_H} - \frac{1}{2\lambda_H} \left(\lambda_{HS} v_S^2 + 2\lambda_H^{\mu e} v_{S^e} v_{S^\mu} + \sum_{\ell} \lambda_{HS^\ell} v_{S^\ell}^2 \right), \\
v_S^2 = & -\frac{1}{\lambda_S} \left(\mu_S^2 + \frac{\lambda_{HS} v^2}{2} + \lambda_S^{\mu e} v_S^e v_S^\mu \right) - \frac{1}{\sqrt{2}\lambda_S v_S} \left(\sum_{\ell} \mu_{\ell\ell} v_{S^\ell}^2 + \tilde{\mu}_{\mu e} v_{S^e} v_{S^\mu} \right), \\
\lambda_{S^e} v_{S^e}^3 = & - \left(\mu_{S^e}^2 + \frac{\lambda_{\mu e} + 2\lambda'_{\mu e}}{2} v_{S^\mu}^2 + \frac{\lambda_{HS^e}}{2} v^2 + \sqrt{2}\mu_{ee} v_S + \frac{3\lambda_{S^e}^{\mu e}}{2} v_{S^e} v_{S^\mu} \right) v_{S^e} \\
& - \frac{1}{2} \left(\lambda_S^{\mu e} v_S^2 + \lambda_H^{\mu e} v^2 + 2\mu_{\mu e}^2 + \sqrt{2}\tilde{\mu}_{\mu e} v_S + \lambda_{S^\mu}^{\mu e} v_{S^\mu}^2 \right) v_{S^\mu}, \\
\lambda_{S^\mu} v_{S^\mu}^3 = & - \left(\mu_{S^\mu}^2 + \frac{\lambda_{\mu e} + 2\lambda'_{\mu e}}{2} v_{S^e}^2 + \frac{\lambda_{HS^\mu}}{2} v^2 + \sqrt{2}v_S \mu_{\mu\mu} + \frac{3\lambda_{S^\mu}^{\mu e}}{2} v_{S^e} v_{S^\mu} \right) v_{S^\mu} \\
& - \frac{1}{2} \left(\lambda_S^{\mu e} v_S^2 + \lambda_H^{\mu e} v^2 + 2\mu_{\mu e}^2 + \sqrt{2}\tilde{\mu}_{\mu e} v_S + \lambda_{S^e}^{\mu e} v_{S^e}^2 \right) v_{S^e}, \quad (8)
\end{aligned}$$

where we have used $\partial V/\partial v_i = 0$ with $v_i = v, v_S$, and v_{S^ℓ} . In addition, the symmetric scalar mass-square matrix is obtained as:

$$m_S^2 = \begin{pmatrix} m_{S^e}^2 & m_{s^e s^\mu}^2 & m_{s^e \phi}^2 & m_{s^e s}^2 \\ m_{s^e s^\mu}^2 & m_{S^\mu}^2 & m_{s^\mu \phi}^2 & m_{s^\mu s}^2 \\ m_{s^e \phi}^2 & m_{s^\mu \phi}^2 & m_\phi^2 & m_{\phi s}^2 \\ m_{s^e s}^2 & m_{s^\mu s}^2 & m_{\phi s}^2 & m_S^2 \end{pmatrix}, \quad (9)$$

where the matrix elements are obtained as:

$$\begin{aligned}
m_{S^e}^2 &= 2\lambda_{S^e}v_{S^e}^2 + \frac{3}{2}\lambda_{S^e}^{\mu e}v_{S^e}v_{S^\mu} \\
&\quad - \frac{1}{2}\left(\lambda_S^{\mu e}v_S^2 + \lambda_H^{\mu e}v^2 + \lambda_{S^\mu}^{\mu e}v_{S^\mu}^2 + 2\mu_{\mu e}^2 + \sqrt{2}\tilde{\mu}_{\mu e}v_S\right)\frac{v_{S^\mu}}{v_{S^e}}, \\
m_{S^\mu}^2 &= 2\lambda_{S^\mu}v_{S^\mu}^2 + \frac{3}{2}\lambda_{S^\mu}^{\mu e}v_{S^e}v_{S^\mu} \\
&\quad - \frac{1}{2}\left(\lambda_S^{\mu e}v_S^2 + \lambda_H^{\mu e}v^2 + \lambda_{S^e}^{\mu e}v_{S^e}^2 + 2\mu_{\mu e}^2 + \sqrt{2}\tilde{\mu}_{\mu e}v_S\right)\frac{v_{S^e}}{v_{S^\mu}}, \\
m_\phi^2 &= 2v^2\lambda_H, \quad m_S^2 = 2\lambda_Sv_S^2 - \frac{1}{\sqrt{2}v_S}\left(\sum_\ell \mu_{\ell\ell}v_{S^\ell}^2 + \tilde{\mu}_{\mu e}v_{S^e}v_{S^\mu}\right), \\
m_{s^e s^\mu}^2 &= (2\lambda_{S^e}v_{S^e}^2 - m_{S^e}^2)\frac{v_{S^e}}{v_{S^\mu}} + (\lambda_{\mu e} + 2\lambda'_{\mu e})v_{S^e}v_{S^\mu} + \frac{3}{2}\sum_\ell \lambda_{S^\ell}^{\mu e}v_{S^\ell}^2, \\
m_{s^\ell\phi}^2 &= (\lambda_H^{\mu e}r_v + \lambda_{HS^\ell})vv_{S^\ell}, \quad m_{\phi S}^2 = \lambda_{HS}vv_S, \\
m_{s^{e(\mu)}S}^2 &= \sqrt{2}\mu_{ee(\mu\mu)}v_{S^{e(\mu)}} + \left(\lambda_S^{\mu e}v_S + \frac{\tilde{\mu}_{\mu e}}{\sqrt{2}}\right)v_{S^{\mu(e)}}. \tag{10}
\end{aligned}$$

In $m_{s^\ell\phi}^2$, $r_v^\ell = v_{S^\mu}/v_{S^e}(v_{S^e}/v_{S^\mu})$ for $\ell = e(\mu)$. The relations in Eq. (8) have been applied to $m_{S^\ell}^2$, m_ϕ^2 , and m_S^2 .

To explain the anomalous lepton $g-2$, we numerically find that $m_{S^\ell} < 100$ GeV, $v_{S^\ell} \lesssim 1$ GeV, and $(\lambda_H^{\mu e}, \lambda_{HS^\ell}) \gtrsim 0$ are preferred in the model. In addition, to fit the neutrino data, we need $\mu_{\mu e}^2 \ll v^2$ when the Yukawa couplings are taken to be of $O(10^{-5} - 10^{-4})$. Thus, the positive v , v_{S,S^ℓ} , and $m_{S^\ell,\phi,S}^2$ can be achieved when the parameters are taken to follow the conditions:

$$\begin{aligned}
\lambda_{H,S,S^\ell} &> 0, \quad \mu_{H,S^\ell,S}^2 > 0, \quad \mu_S^2 + \frac{\lambda_{HS}v^2}{2} < 0, \quad \lambda_{HS} < 0, \\
\lambda_S^{\mu e} &< 0, \quad 0 < 2\mu_{\mu e}^2 + \lambda_{HS^\ell}v^2 < -(\lambda_S^{\mu e}v_S^2 + \lambda_H^{\mu e}v^2 + \sqrt{2}\tilde{\mu}_{\mu e}v_S). \tag{11}
\end{aligned}$$

In addition, in order to avoid the strict constraint from the precision Higgs measurements, $m_{s^\ell\phi}^2 \ll m_\phi^2$ is necessary; that is,

$$(\lambda_H^{\mu e}r_v^\ell + \lambda_{HS^\ell})v_{S^\ell} \ll 2v\lambda_H. \tag{12}$$

Using these conditions, it can be found that with $|\lambda_{HS}| < 1$, the scalar ϕ can approximate the SM Higgs h with a mass of $m_h = 125$ GeV.

After $U(1)_{e-\mu}$ symmetry is spontaneously broken, the associated Z' -gauge boson becomes a massive particle and its mass can be obtained as:

$$m_{Z'} = g_{Z'} \sqrt{v_\eta^2 + 4v_S^2 + v_{S^e}^2 + v_{S^\mu}^2}, \quad (13)$$

where $g_{Z'}$ is $U(1)_{e-\mu}$ gauge coupling constant.

III. CHARGED LEPTON AND NEUTRINO MASS MATRICES

From Eq. (3), it can be seen that with the exception of the τ -lepton, the electron and muon do not directly obtain their masses with the Higgs mechanism. Nevertheless, their masses can be induced through the mixings with $X_{L,R}^\ell$ and $X_{L,R}$, where the Feynman diagrams are shown in Fig. 1.

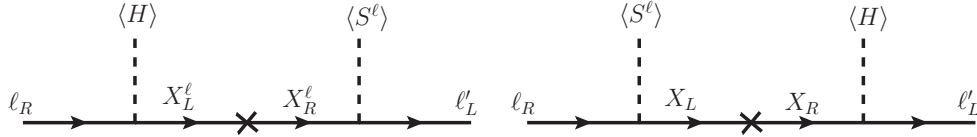


FIG. 1: Feynman diagrams used to induce the electron and muon masses.

Using the Yukawa couplings and the VEVs of scalar fields, the 6×6 charged lepton mass matrix in the flavor basis of $(e, \mu, \tau, X^e, X^\mu, X)_{L,R}$ is written as:

$$M_{CL} = \begin{pmatrix} 0 & 0 & 0 & m_{eX^e} & m_{eX^\mu} & m_{eX} \\ 0 & 0 & 0 & m_{\mu X^e} & m_{\mu X^\mu} & m_{\mu X} \\ 0 & 0 & m_\tau^0 & m_{\tau X^e} & m_{\tau X^\mu} & m_{\tau X} \\ m_{X^e e} & 0 & 0 & M_{X^e} & 0 & 0 \\ 0 & m_{X^\mu \mu} & 0 & 0 & M_{X^\mu} & 0 \\ m_{X^e} & m_{X^\mu} & 0 & 0 & 0 & M_X \end{pmatrix}, \quad (14)$$

where the matrix elements are given as:

$$\begin{aligned} m_{\ell' X^\ell} &= \frac{y_{\ell'}^\ell v_{S^\ell}}{\sqrt{2}}, \quad m_{\ell' X} = \frac{\tilde{y}_{\ell'} v}{\sqrt{2}}, \\ m_{X^\ell \ell} &= \frac{y_X^\ell v}{\sqrt{2}}, \quad m_{X \ell} = \frac{y_\ell v_{S^\ell}}{\sqrt{2}}. \end{aligned} \quad (15)$$

Since several phenomena are related to $m_{\ell'X^\ell(X)}$ and $m_{X^\ell(X)\ell}$, we thus use them as the free parameters instead of the corresponding Yukawa couplings and VEVs. In this study, we assume that the relevant Yukawa couplings are real parameters. The mass matrix M_{CL} can be diagonalized by the unitary matrices $U_{L,R}$ as $M_{CL}^{\text{diag}} = U_L M_{CL} U_R^\dagger$. The m_ℓ eigenvalues can be obtained using $M_{CL}^{\text{diag}} M_{CL}^{\text{diag}\dagger} = U_L M_{CL} M_{CL}^\dagger U_L^\dagger$ and $M_{CL}^{\text{diag}\dagger} M_{CL}^{\text{diag}} = U_R M_{CL}^\dagger M_{CL} U_R^\dagger$.

Although the right-handed neutrinos N^ℓ are introduced, since the left-handed SM leptons do not carry the $U(1)_{e-\mu}$ charges, the neutrino mass cannot be generated at the tree-level in the model. Nonetheless, the neutrino mass can be produced through the radiative effects, for which the Feynman diagrams are shown in Fig. 2.

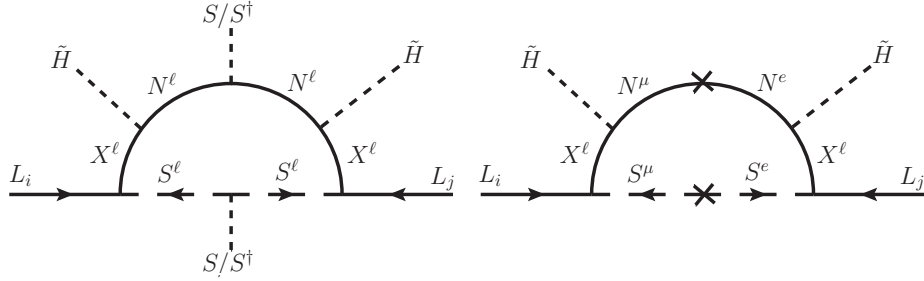


FIG. 2: Feynman diagrams used to generate the neutrino masses.

Using the Yukawa and scalar couplings shown in Eq. (3) and Eq. (6), respectively, the loop-induced neutrino mass matrix elements, denoted as $\nu_j^T C m_{ji}^\nu \nu_i$, can be obtained as:

$$m_{ji}^\nu = \frac{v v_S^2}{\sqrt{2}(4\pi)^2} \sum_{\ell=e,\mu} \frac{\mu_{\ell\ell} m_{N^\ell} (\tilde{y}_X^\ell)^2}{m_{X^\ell}^4} \frac{m_{jX^\ell} m_{iX^\ell}}{(v_{S^\ell})^2} J_0 \left(\frac{m_{S^\ell}^2}{m_{X^\ell}^2}, \frac{m_{N^\ell}^2}{m_{X^\ell}^2} \right) - \frac{\tilde{y}_X^e \tilde{y}_X^\mu v^2 \mu_{\mu e}^2 m_{N_{\mu e}}}{(4\pi)^2 v_{S^e} v_{S^\mu}} \frac{(m_{jX^\mu} m_{iX^\mu} + m_{jX^\mu} m_{iX^e})}{m_{X^\ell}^4} J_1 \left(\frac{m_{S^\ell}^2}{m_{X^\ell}^2}, \frac{m_{N^\mu}^2}{m_{X^\ell}^2}, \frac{m_{N^e}^2}{m_{X^\ell}^2} \right), \quad (16)$$

where the Latin letters j, i denote the active neutrino flavors, and the first (second) term originates from the left (right) panel in Fig. 2. For simplicity, we take $m_{S^e} = m_{S^\mu} = m_{S^\ell}$ and $m_{X^e} = m_{X^\mu} = m_{X^\ell}$; $m_{N^\ell} = h_\ell v_S / \sqrt{2}$ and $m_{\ell'X^\ell(X)}$ defined in Eq. (15) are used, and the loop integrals are expressed as:

$$J_0(a, b) = \int_0^1 dx \int_0^x dy \frac{(1-x)(x-y)}{(1+(a-1)x+(b-a)y)^2},$$

$$J_1(a, b, c) = \int_0^1 dx \int_0^x dy \int_0^y dz \frac{(1-x)(x-y)}{(1+(a-1)x+(b-a)y+(c-a)z)^3}. \quad (17)$$

The neutrino mass matrix can be diagonalized by the Pontecorvo-Maki-Nakagawa-Sakata (PMNS) matrix as:

$$m_{ij}^\nu = U_{MNS}^* m_\nu^{\text{diag}} U_{MNS}^\dagger, \quad (18)$$

where $m_\nu^{\text{diag}} = \text{diag}(m_1, m_2, m_3)$, and the PMNS matrix can be parametrized as [2]:

$$U_{\text{MNS}} = \begin{pmatrix} c_{12}c_{13} & s_{12}c_{13} & s_{13}e^{-i\delta} \\ -s_{12}c_{23} - c_{12}s_{23}s_{13}e^{i\delta} & c_{12}c_{23} - s_{12}s_{23}s_{13}e^{i\delta} & s_{23}c_{13} \\ s_{12}s_{23} - c_{12}c_{23}s_{13}e^{i\delta} & -c_{12}s_{23} - s_{12}c_{23}s_{13}e^{i\delta} & c_{23}c_{13} \end{pmatrix} \\ \times \text{diag}(1, e^{i\alpha_{21}/2}, e^{i\alpha_{31}/2}), \quad (19)$$

with $s_{ij} \equiv \sin \theta_{ij}$ and $c_{ij} \equiv \cos \theta_{ij}$. δ is the Dirac CP violating phase, and $\alpha_{21,31}$ are Majorana CP violating phases.

IV. $\ell' \rightarrow \ell\gamma$, AND LEPTON $g-2$

If we add the couplings $H^\dagger H S^{\ell^\dagger} S^\ell$ and $H^\dagger H S^e S^\mu$ to Fig. 1, it can be seen that the radiative LFV processes can be induced through the loop effects, for which the relevant Feynman diagrams are sketched in Fig. 3. The current experimental upper limits on the BR for the relevant LFV processes are given as [2]:

$$\begin{aligned} BR(\mu \rightarrow e\gamma) &< 4.2 \times 10^{-13}, \\ BR(\tau \rightarrow e\gamma) &< 3.3 \times 10^{-8}, \\ BR(\tau \rightarrow \mu\gamma) &< 4.4 \times 10^{-8}. \end{aligned} \quad (20)$$

Since the radiative LFV processes are dominant in the model, we skip the analysis for the subleading $\mu \rightarrow 3e$ and $\tau \rightarrow 3\ell$ decays.

Using the Yukawa and scalar couplings, the effective interactions for $\ell' \rightarrow \ell\gamma$ can be written as:

$$\mathcal{L}_{\ell' \rightarrow \ell\gamma} = \frac{e}{2} m_{\ell'} \bar{\ell} \sigma_{\mu\nu} \left(T_L^{\ell'\ell} P_L + T_R^{\ell'\ell} P_R \right) \ell' F^{\mu\nu}, \quad (21)$$

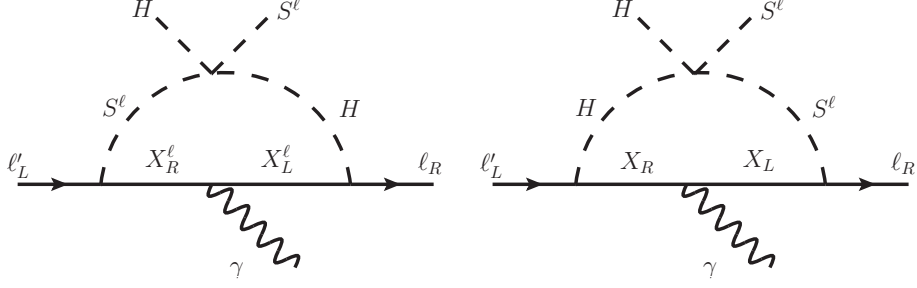


FIG. 3: Selected Feynman diagrams for the $\ell' \rightarrow \ell\gamma$ decays.

where the Wilson coefficients in the model are obtained as:

$$\begin{aligned}
T_L^{\mu e} &= \frac{\lambda_{HS^e} + \lambda_H^{\mu e} r_v^e}{2m_\mu(4\pi)^2} \left[\frac{m_{\mu X^e} m_{X^e e}}{m_{X^\ell}^3} J_2 \left(\frac{m_{S^\ell}^2}{m_{X^\ell}^2}, \frac{m_\phi^2}{m_{X^\ell}^2} \right) + \frac{m_{\mu X} m_{X^e}}{m_X^3} J_2 \left(\frac{m_{S^\ell}^2}{m_X^2}, \frac{m_\phi^2}{m_X^2} \right) \right], \\
T_R^{\mu e} &= \frac{\lambda_{HS^\mu} + \lambda_H^{\mu e} r_v^\mu}{2m_\mu(4\pi)^2} \left[\frac{m_{eX^\mu} m_{X^\mu \mu}}{m_{X^\ell}^3} J_2 \left(\frac{m_{S^\ell}^2}{m_{X^\ell}^2}, \frac{m_\phi^2}{m_{X^\ell}^2} \right) + \frac{m_{eX} m_{X^\mu}}{m_X^3} J_2 \left(\frac{m_{S^\ell}^2}{m_X^2}, \frac{m_\phi^2}{m_X^2} \right) \right], \\
T_L^{\tau \ell} &= \frac{\lambda_{HS^\ell} + \lambda_H^{\mu e} r_v^\ell}{2m_\tau(4\pi)^2} \left[\frac{m_{\tau X^\ell} m_{X^\ell \ell}}{m_{X^\ell}^3} J_2 \left(\frac{m_{S^\ell}^2}{m_{X^\ell}^2}, \frac{m_\phi^2}{m_{X^\ell}^2} \right) + \frac{m_{\tau X} m_{X^\ell}}{m_X^3} J_2 \left(\frac{m_{S^\ell}^2}{m_X^2}, \frac{m_\phi^2}{m_X^2} \right) \right], \quad (22)
\end{aligned}$$

$T_R^{\tau \ell} = 0$, and the loop integral J_2 is defined by:

$$J_2(a, b) = \int_0^1 dx_1 \int_0^{x_1} dx_2 \int_0^{x_2} dx_3 \frac{1 - x_2}{(1 + (a - 1)x_2 + (b - a)x_3)^2}. \quad (23)$$

The definitions shown in Eq. (15) have been used. Due to $m_\ell \ll m_{\ell'}$, we have neglected the m_ℓ effects. As a result, the BR for the $\ell' \rightarrow \ell\gamma$ decay can be written as:

$$BR(\ell' \rightarrow \ell\gamma) = \tau_{\ell'} \frac{\alpha m_{\ell'}^5}{4} \left(|T_L^{\ell' \ell}|^2 + |T_R^{\ell' \ell}|^2 \right). \quad (24)$$

In order to satisfy the current upper limit of $BR^{\text{exp}}(\mu \rightarrow e\gamma) < 4.2 \times 10^{-13}$, one can take $m_{\mu X^e} \approx m_{eX^\mu} \approx 0$ or the conditions assumed as:

$$\begin{aligned}
\frac{m_{\mu X^e} m_{X^e e}}{m_{X^\ell}^3} J_2 \left(\frac{m_{S^\ell}^2}{m_{X^\ell}^2}, \frac{m_\phi^2}{m_{X^\ell}^2} \right) &\approx -\frac{m_{\mu X} m_{X^e}}{m_X^3} J_2 \left(\frac{m_{S^\ell}^2}{m_X^2}, \frac{m_\phi^2}{m_X^2} \right), \\
\frac{m_{eX^\mu} m_{X^\mu \mu}}{m_{X^\ell}^3} J_2 \left(\frac{m_{S^\ell}^2}{m_{X^\ell}^2}, \frac{m_\phi^2}{m_{X^\ell}^2} \right) &\approx -\frac{m_{eX} m_{X^\mu}}{m_X^3} J_2 \left(\frac{m_{S^\ell}^2}{m_X^2}, \frac{m_\phi^2}{m_X^2} \right). \quad (25)
\end{aligned}$$

In this study, we adopt the latter requirements shown in Eq. (25). Hence, in the numerical analysis, we only focus on the $\tau \rightarrow \ell\gamma$ decays.

It is known that the radiative quantum corrections to a lepton current can be expressed as:

$$\Gamma^\alpha = \bar{\ell}(p') \left[\gamma^\alpha F_1(k^2) + \frac{i\sigma^{\alpha\beta} k_\beta}{2m_\ell} F_2(k^2) \right] \ell(p), \quad (26)$$

where the lepton $g - 2$ can be defined by:

$$a_\ell = \frac{g_\ell - 2}{2} = F_2(0). \quad (27)$$

Using this definition, the lepton $g - 2$ can be induced by Fig. 3 with $\ell' = \ell$. Based on the results shown in Eq. (22), the lepton $g - 2$ can be formulated as:

$$\delta a_\ell = m_\ell \frac{\lambda_{HS^\ell} + \lambda_H^{\mu e} r_v^\ell}{(4\pi)^2} \left[\frac{m_{\ell X^\ell} m_{X^\ell \ell}}{m_{X^\ell}^3} J_2 \left(\frac{m_{S^\ell}^2}{m_{X^\ell}^2}, \frac{m_\phi^2}{m_{X^\ell}^2} \right) + \frac{m_{\ell X} m_{X \ell}}{m_X^3} J_2 \left(\frac{m_{S^\ell}^2}{m_X^2}, \frac{m_\phi^2}{m_X^2} \right) \right]. \quad (28)$$

It can be seen that the obtained δa_μ is proportional to m_ℓ and linearly depends on $\lambda_{HS^\ell} + \lambda_H^{\mu e} r_v^\ell$, which is related to $m_{s^\ell \phi}^2$. Since λ_{HS^ℓ} and $\lambda_H^{\mu e}$ are free parameters, to use fewer scanned parameters, for simplicity, we take $\lambda_H^{\mu e} = 0$ in our numerical analysis.

As mentioned in the introduction, the Z' -gauge boson can contribute to the lepton $g - 2$, and the result can be formulated as:

$$\delta a_\ell^{Z'} = \frac{g_{Z'}^2 r_\ell^2}{16\pi^2} \int_0^1 dx \frac{x(1-x)(2x-4) - 2r_\ell^2 x^3}{(1-x)(1-r_\ell^2 x) + r_\ell^2 x}, \quad (29)$$

with $r_\ell = m_\ell/m_{Z'}$. Due to the fact that $2x - 4 < 0$ in the integral, the resulting $\delta a_\ell^{Z'}$ is always negative. Because $\delta a_e^{Z'}/\delta a_\mu^{Z'} \approx m_e^2/m_\mu^2 \approx 2.4 \times 10^{-5}$, if $\delta a_e^{Z'} \sim -5 \times 10^{-13}$ is taken, we obtain $\delta a_\mu^{Z'} \sim -2.1 \times 10^{-8}$. However, the large negative $\delta a_\mu^{Z'}$ contradicts to the current data, and the sign cannot be flipped via other effects in the model. To avoid this issue, we can take proper values for $g_{Z'}$ and $m_{Z'}$ to suppress $\delta a_\mu^{Z'}$. For instance, with $g_{Z'} \sim 5 \times 10^{-4}$ and $m_{Z'} \sim 1$ GeV, we have $\delta a_\mu^{Z'} \sim -2.3 \times 10^{-11}$; thus, the result will not affect the contributions from Eq. (28).

V. NUMERICAL ANALYSIS

A. Constraints and setting the scanned parameter regions

Since m_e and m_μ are induced through the diagonalization of the 6×6 M_{CL} matrix, basically, the parameters in M_{CL} have to obtain $m_e \sim 5.1 \times 10^{-4}$ GeV and $m_\mu \sim 0.105$ GeV. However, the parameter scan is inefficient when we fit the mass hierarchy between the electron and the muon. In order to obtain more allowed sampling points, we take $m_e = (8, 4) \times 10^{-4}$ GeV and $m_\mu = (0.107, 0.103)$ GeV as the constraints.

Although the neutrino mass order is not yet determined, since other analyses are not sensitive to the mass order, we use the normal ordering (NO) scheme, i.e. $m_1 < m_2 \ll m_3$,

in our study. Based on the neutrino oscillation data [2], the central values of θ_{ij} , δ , and $\Delta m_{ij}^2 = m_i^2 - m_j^2$ using the global fit can then be obtained as [65]:

$$\begin{aligned}\theta_{12} &= 34.5^\circ, \quad \theta_{23} = 47.7^\circ, \quad \theta_{13} = 8.45^\circ, \quad \delta = 218^\circ, \\ \Delta m_{21}^2 &= 7.55 \times 10^{-5} \text{ eV}^2, \quad \Delta m_{31}^2 = 2.50 \times 10^{-3} \text{ eV}^2,\end{aligned}\quad (30)$$

where $m_1 = 0$ is used, and the Majorana phases are taken to be $\alpha_{21(31)} = 0$. Using the 3σ uncertainties that are shown in [65] and the relation shown in Eq. (18), the $|m_{ji}^\nu|$ ranges in units of eV can be estimated as:

$$\begin{pmatrix} |m_{ee}^\nu| & |m_{e\mu}^\nu| & |m_{e\tau}^\nu| \\ |m_{\mu e}^\nu| & |m_{\mu\mu}^\nu| & |m_{\mu\tau}^\nu| \\ |m_{\tau e}^\nu| & |m_{\tau\mu}^\nu| & |m_{\tau\tau}^\nu| \end{pmatrix}_{\text{NO}} \simeq \begin{pmatrix} 0.11 - 0.45 & 0.12 - 0.82 & 0.12 - 0.82 \\ 0.12 - 0.82 & 2.4 - 3.3 & 2.0 - 2.2 \\ 0.12 - 0.82 & 2.0 - 2.2 & 2.2 - 3.1 \end{pmatrix} \times 10^{-2} \text{ eV}. \quad (31)$$

We thus use the results in Eq. (31) as the inputs to constrain the free parameters.

In order to scan the free parameters and obtain the allowed parameter regions when the considered constraints are satisfied, we choose the parameters in units of GeV from the Yukawa sector as:

$$\begin{aligned}m_{eX^e(eX)} &= (3, 5), \quad m_{eX^\mu, \mu X^e} = (-2, 2), \quad m_{\mu X^\mu} = (2, 10), \\ m_{X^e e} &= (-10, -3), \quad m_{X^\mu \mu} = (20, 50), \quad m_{X^e} = (3, 10), \\ m_{N_{\mu e}} &= (-100, 100), \quad m_{\tau X} = (-10, 10), \quad m_{X^\ell} = (600, 1000), \\ m_X &= (800, 1200), \quad m_{N^\mu} = (10, 30), \quad m_{N^e} = (100, 300),\end{aligned}\quad (32)$$

and $m_{\tau X^e, \tau X^\mu} = 2 \text{ GeV}$, whereas $m_{\mu X}$ and m_{X^μ} are determined by Eq. (25). We note that in order to obtain $\delta a_e < 0$ and $\delta a_\mu > 0$, we fix $m_{X^e e} < 0$ and $m_{X^\mu \mu} > 0$. The mass of a vector-like lepton doublet in the range of $120 - 790 \text{ GeV}$ is excluded by the CMS experiment [66] in the multilepton final states at $\sqrt{s} = 13 \text{ TeV}$. Since the $X^\ell - \tau$ mixings are small in our model, the m_{X^ℓ} constraint through the coupling $X^\ell \tau Z$ can be looser. The current upper limit on the vector-like lepton singlet is $m_X \lesssim 176 \text{ GeV}$, which was reported by ATLAS [67]. Hence, the chosen regions for $m_{X^\ell, X}$ follow the current LHC results. The parameter regions from the scalar potential are taken as: $v = 246 \text{ GeV}$, $v_S = 100 \text{ GeV}$, $v_{S^\ell} = 1 \text{ GeV}$, and:

$$\mu_{ee} = (-5, 5) \text{ GeV}, \quad \mu_{\mu\mu} = (-1, 1) \text{ GeV}, \quad \mu_{\mu e} = (-10, 10) \text{ GeV}. \quad (33)$$

The involving dimensionless Yukawa and scalar couplings are set as: $\lambda_{HS^e} = 6$, $\lambda_{HS^\mu} = 8$, $\tilde{y}_X^e = (-2, 2) \times 10^{-5}$, and $\tilde{y}_X^\mu = (-2, 2) \times 10^{-4}$. In addition, in order to obtain the sizable

$\delta a_{e,\mu}$, we require:

$$\begin{aligned}\delta a_e &= (-12.4, -5.2) \times 10^{-13}, \\ \delta a_\mu &> 5 \times 10^{-10}.\end{aligned}\tag{34}$$

B. Numerical analysis and discussion

From Eq. (31), it can be seen that the matrix elements of m_{ji}^ν are similar in terms of order of magnitude; thus, we use 2×10^8 sampling points to scan the relevant parameters. However, to obtain the hierarchical values for m_e and m_μ from the matrix in Eq. (14), we use 10^9 sampling points.

To show that $m_e \sim 5.1 \times 10^{-4}$ GeV and $m_\mu \sim 0.105$ GeV can be achieved in the chosen parameter regions, the correlation between the obtained m_e and m_μ is shown in Fig. 4(a). The correlation between $\delta a_{e(\mu)}$ and m_e can be found in Fig. 4(b), where $\delta a_{e(\mu)}$ is in units of $10^{-13}(10^{-10})$ and m_e is scaled by 10^{-4} , indicated by blue(green) points. It can be seen that when $m_e \sim 5.1 \times 10^{-4}$ GeV is obtained, and the same parameter values can lead to $\delta a_e \sim O(-10^{-12})$ and $\delta a_\mu \sim O(10^{-9})$. For clarity, we also show the correlation between the obtained δa_e and δa_μ in Fig. 5.

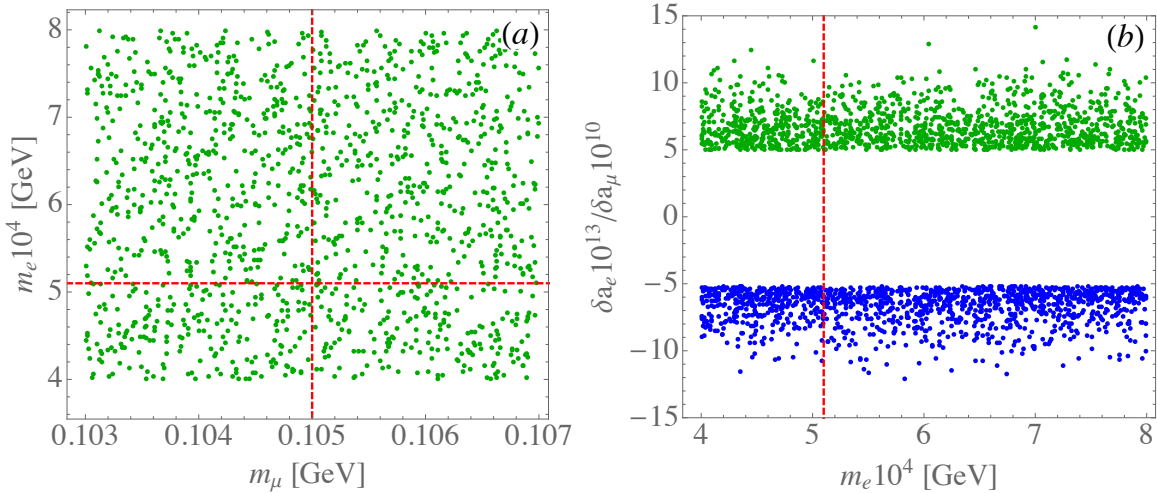


FIG. 4: (a) Correlation between the obtained m_e and m_μ , and (b) correlation between $\delta a_{e(\mu)}$ and m_e , where m_e is scaled by 10^{-4} , and $\delta a_{e(\mu)}$ is in units of $10^{-13}(10^{-10})$, indicated by blue(green) points.

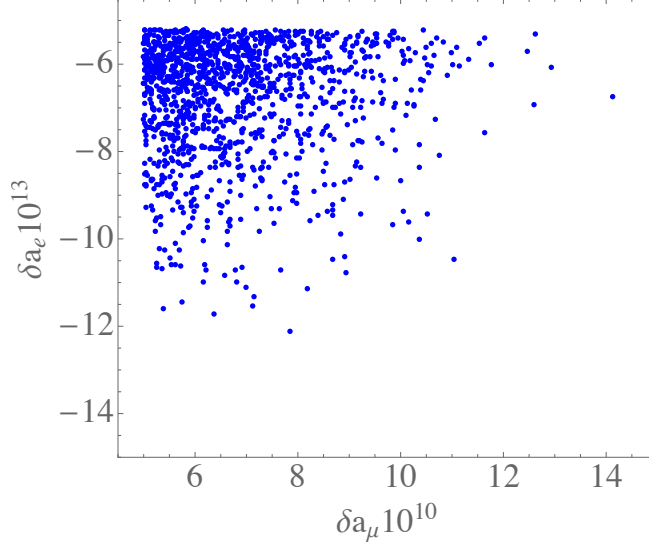


FIG. 5: Correlation between the obtained δa_e and δa_μ .

It is known that M_{CL} in Eq. (14), δa_ℓ in Eq. (28), and m_{ji}^ν in Eq. (16) have common free parameters, such as $m_{\ell X^\ell}$ and $m_{\tau X^\ell}$. To more efficiently obtain the allowed parameter regions, we separately scan the parameters to fit the chosen ranges of m_ℓ and δa_ℓ and the m_{ji}^ν shown in Eq. (31). We demonstrate the scanning results for m_{eX^e} versus $m_{\mu X^\mu}$ in Fig. 6, where the filled circles arise from the constraints shown in Eq. (31), and the squares are derived from the m_ℓ and δa_ℓ constraints. According to the results, the same parameters from the different phenomena can have the common values.

In the numerical analysis, we used the relations in Eq. (25), where the rare radiative $\mu \rightarrow e\gamma$ decay can be basically as small as the current upper limit. We thus focus on the situations in the $\tau \rightarrow \ell\gamma$ decays. Using the allowed parameter regions, which are limited by the selected m_ℓ and δa_ℓ regions, the BRs in units of 10^{-8} for the $\tau \rightarrow \ell\gamma$ decays with respect to δa_e are shown in Fig. 7(a), where the filled circles and triangles denote the $\tau \rightarrow e\gamma$ and $\tau \rightarrow \mu\gamma$ results, respectively. The correlations of $BR(\tau \rightarrow \ell\gamma)$ with δa_μ are given in Fig. 7(b). From the results, it can be clearly seen that when the upper limits of $BR(\tau \rightarrow \ell\gamma)$ are satisfied, δa_e of $O(-10^{-12})$ and δa_μ of $O(10^{-9})$ can be achieved. In addition, it is found that with the constrained parameter regions, the resulting $BR(\tau \rightarrow \mu\gamma)$ can be over the current upper limit; that is, the $\tau \rightarrow \mu\gamma$ decay can further exclude the free parameter space. Nevertheless, when we exclude the sampling points, which are constrained by the $\tau \rightarrow \mu\gamma$

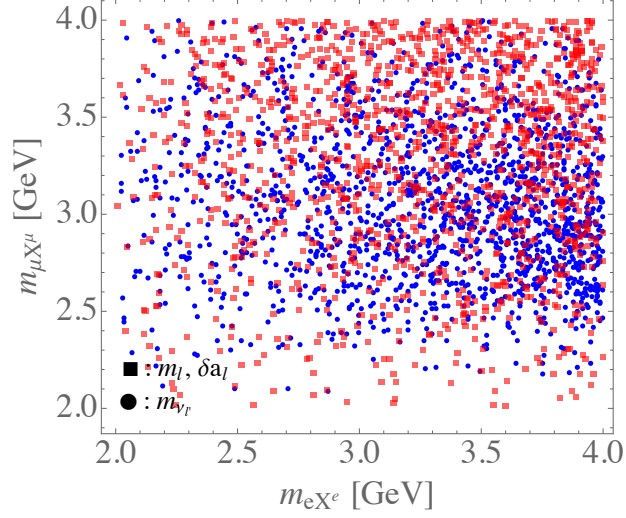


FIG. 6: Resulting correlations for the scanned parameters from different phenomena when they satisfy the chosen ranges, where the filled circles arise from the neutrino data, and the squares are derived from the selected m_ℓ and δa_ℓ ranges.

decay, the δa_ℓ results are not changed.

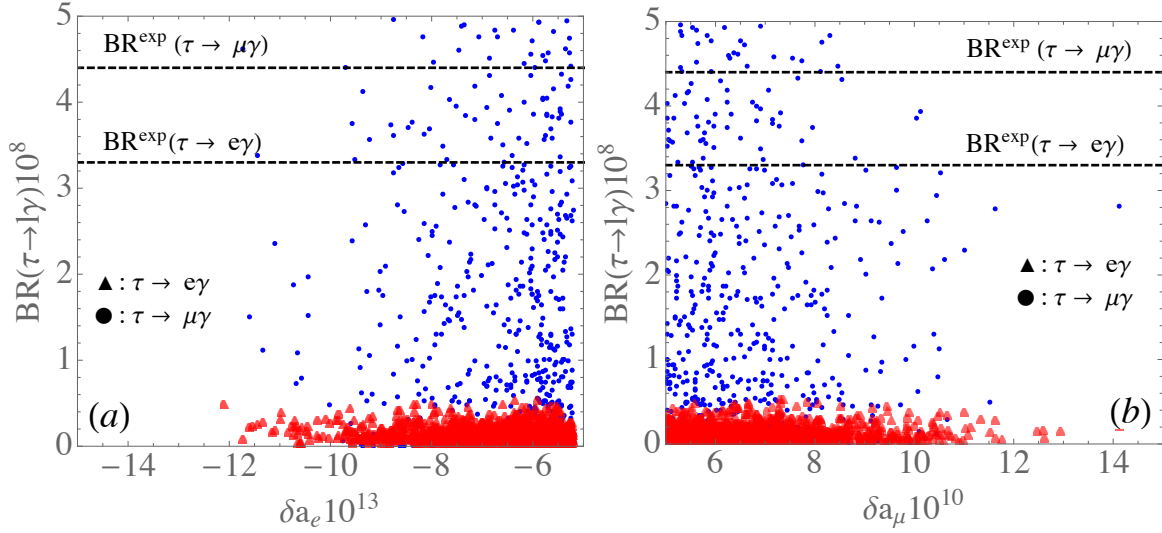


FIG. 7: Correlations of $BR(\tau \rightarrow \ell \gamma)$ (in units of 10^{-8}) with δa_e (left panel) and δa_μ (right panel).

VI. SUMMARY

A gauged $U(1)_{e-\mu}$ extension of the SM is used to explain the electron and muon $g - 2$, where two vector-like lepton doublets, three vector-like lepton singlets, and three scalar singlets are included. Intriguingly, when two Majorana fermions and one scalar singlet are further included, it is found that the neutrino masses can be generated through the radiative seesaw mechanism.

Although the electron and muon do not obtain their masses via the Higgs mechanism, their masses can be induced through mixing with the introduced heavy charged leptons. We found that the mass hierarchy between the electron and the muon can be accommodated in the model. When the bounds of the electron and muon masses and the neutrino data are satisfied, we found that the electron $g - 2$ can reach an order of -10^{-12} , and the muon $g - 2$ can be of an $O(10^{-9})$.

The radiative lepton-flavor violation processes can arise from similar Feynman diagrams, which are used for producing the lepton $g - 2$. When the $\mu \rightarrow e\gamma$ decay is suppressed, and the constrained parameter values are applied, the result of $BR(\tau \rightarrow e\gamma) \lesssim 10^{-8}$ can be obtained. With the same constrained parameter set, we found that the resulting $BR(\tau \rightarrow \mu\gamma)$ can be larger than its current upper limit; that is, the $\tau \rightarrow \mu\gamma$ decay indeed can be used to further constrain the parameter space. Nevertheless, the parameter regions excluded by the $\tau \rightarrow \mu\gamma$ decay do not change the regions allowed for δa_e and δa_μ .

Acknowledgments

We would like to thank Dr. Di Liu for useful comments. This work was supported by the Ministry of Science and Technology of Taiwan, under grants MOST-108-2112-M-006-003-MY2.

-
- [1] G. W. Bennett *et al.* [Muon $g-2$ Collaboration], Phys. Rev. D **73**, 072003 (2006) [hep-ex/0602035].
 - [2] M. Tanabashi *et al.* (Particle Data Group), Phys. Rev. D **98**, 030001 (2018).

- [3] M. Davier, A. Hoecker, B. Malaescu and Z. Zhang, Eur. Phys. J. C **80**, no. 3, 241 (2020) [arXiv:1908.00921 [hep-ph]].
- [4] T. Blum *et al.* [RBC and UKQCD Collaborations], Phys. Rev. Lett. **121**, no. 2, 022003 (2018) [arXiv:1801.07224 [hep-lat]].
- [5] A. Keshavarzi, D. Nomura and T. Teubner, Phys. Rev. D **97**, no. 11, 114025 (2018) [arXiv:1802.02995 [hep-ph]].
- [6] A. Czarnecki and W. J. Marciano, Phys. Rev. D **64**, 013014 (2001) [hep-ph/0102122].
- [7] S. N. Gninenko and N. V. Krasnikov, Phys. Lett. B **513**, 119 (2001) [hep-ph/0102222].
- [8] E. Ma and M. Raidal, Phys. Rev. Lett. **87**, 011802 (2001) Erratum: [Phys. Rev. Lett. **87**, 159901 (2001)] [hep-ph/0102255].
- [9] C. H. Chen and C. Q. Geng, Phys. Lett. B **511**, 77 (2001) [hep-ph/0104151].
- [10] E. Ma, D. P. Roy and S. Roy, Phys. Lett. B **525**, 101 (2002) [hep-ph/0110146].
- [11] B. P. Padley, K. Sinha and K. Wang, Phys. Rev. D **92**, no. 5, 055025 (2015) [arXiv:1505.05877 [hep-ph]].
- [12] R. Benbrik, C. H. Chen and T. Nomura, Phys. Rev. D **93**, no. 9, 095004 (2016) [arXiv:1511.08544 [hep-ph]].
- [13] T. Nomura and H. Okada, Phys. Lett. B **756**, 295 (2016) [arXiv:1601.07339 [hep-ph]].
- [14] S. Baek, T. Nomura and H. Okada, Phys. Lett. B **759**, 91 (2016) [arXiv:1604.03738 [hep-ph]].
- [15] W. Altmannshofer, M. Carena and A. Crivellin, Phys. Rev. D **94**, no. 9, 095026 (2016) [arXiv:1604.08221 [hep-ph]].
- [16] C. H. Chen, T. Nomura and H. Okada, Phys. Rev. D **94**, no. 11, 115005 (2016) [arXiv:1607.04857 [hep-ph]].
- [17] S. Lee, T. Nomura and H. Okada, Nucl. Phys. B **931**, 179 (2018) [arXiv:1702.03733 [hep-ph]].
- [18] C. H. Chen, T. Nomura and H. Okada, Phys. Lett. B **774**, 456 (2017) [arXiv:1703.03251 [hep-ph]].
- [19] A. Das, T. Nomura, H. Okada and S. Roy, Phys. Rev. D **96**, no. 7, 075001 (2017) [arXiv:1704.02078 [hep-ph]].
- [20] K. Kowalska and E. M. Sessolo, JHEP **1709**, 112 (2017) [arXiv:1707.00753 [hep-ph]].
- [21] L. Calibbi, R. Ziegler and J. Zupan, JHEP **1807**, 046 (2018) [arXiv:1804.00009 [hep-ph]].
- [22] B. Barman, D. Borah, L. Mukherjee and S. Nandi, Phys. Rev. D **100**, no. 11, 115010 (2019) [arXiv:1808.06639 [hep-ph]].

- [23] C. H. Chen and T. Nomura, Phys. Rev. D **100**, no. 1, 015024 (2019) [arXiv:1903.03380 [hep-ph]].
- [24] T. Nomura and H. Okada, arXiv:1903.05958 [hep-ph].
- [25] C. H. Chen and T. Nomura, JHEP **1910**, 005 (2019) [arXiv:1906.10516 [hep-ph]].
- [26] J. Cao, J. Lian, L. Meng, Y. Yue and P. Zhu, arXiv:1912.10225 [hep-ph].
- [27] C. H. Chen and T. Nomura, arXiv:2001.07515 [hep-ph].
- [28] S. Iguro, Y. Omura and M. Takeuchi, arXiv:2002.12728 [hep-ph].
- [29] N. Kumar, T. Nomura and H. Okada, arXiv:2002.12218 [hep-ph].
- [30] J. Kawamura, S. Okawa and Y. Omura, arXiv:2002.12534 [hep-ph].
- [31] C. Han, M. L. López-Ibañez, A. Melis, Ó. Vives, L. Wu and J. M. Yang, arXiv:2003.06187 [hep-ph].
- [32] A. S. de Jesus, S. Kovalenko, F. S. Queiroz, C. A. d. S. Pires and Y. S. Villamizar, arXiv:2003.06440 [hep-ph].
- [33] S. Borsanyi *et al.*, arXiv:2002.12347 [hep-lat].
- [34] A. Crivellin, M. Hoferichter, C. A. Manzari and M. Montull, arXiv:2003.04886 [hep-ph].
- [35] J. Grange *et al.* [Muon g-2 Collaboration], arXiv:1501.06858 [physics.ins-det].
- [36] M. Otani [E34 Collaboration], JPS Conf. Proc. **8**, 025008 (2015).
- [37] T. Aoyama, M. Hayakawa, T. Kinoshita and M. Nio, Phys. Rev. D **91**, no. 3, 033006 (2015)
Erratum: [Phys. Rev. D **96**, no. 1, 019901 (2017)] [arXiv:1412.8284 [hep-ph]].
- [38] T. Aoyama, T. Kinoshita, and M. Nio, Atoms **7**, 28 (2019).
- [39] R. H. Parker, C. Yu, W. Zhong, B. Estey, H. Müller, Science **360**, 191 (2018).
- [40] G. F. Giudice, P. Paradisi and M. Passera, JHEP **1211**, 113 (2012) [arXiv:1208.6583 [hep-ph]].
- [41] A. Aboubrahim, T. Ibrahim and P. Nath, Phys. Rev. D **89**, no. 9, 093016 (2014)
[arXiv:1403.6448 [hep-ph]].
- [42] A. Abada, V. De Romeri and A. M. Teixeira, JHEP **1409**, 074 (2014) [arXiv:1406.6978 [hep-ph]].
- [43] A. Aboubrahim, T. Ibrahim and P. Nath, Phys. Rev. D **94**, no. 1, 015032 (2016)
[arXiv:1606.08336 [hep-ph]].
- [44] W. J. Marciano, A. Masiero, P. Paradisi and M. Passera, Phys. Rev. D **94**, no. 11, 115033 (2016) [arXiv:1607.01022 [hep-ph]].
- [45] H. Davoudiasl and W. J. Marciano, Phys. Rev. D **98**, no. 7, 075011 (2018) [arXiv:1806.10252

- [hep-ph]].
- [46] A. Crivellin, M. Hoferichter and P. Schmidt-Wellenburg, Phys. Rev. D **98**, no. 11, 113002 (2018) [arXiv:1807.11484 [hep-ph]].
 - [47] J. Liu, C. E. M. Wagner and X. P. Wang, JHEP **1903**, 008 (2019) [arXiv:1810.11028 [hep-ph]].
 - [48] X. F. Han, T. Li, L. Wang and Y. Zhang, Phys. Rev. D **99**, no. 9, 095034 (2019) [arXiv:1812.02449 [hep-ph]].
 - [49] M. Endo and W. Yin, JHEP **1908**, 122 (2019) [arXiv:1906.08768 [hep-ph]].
 - [50] M. Abdullah, B. Dutta, S. Ghosh and T. Li, Phys. Rev. D **100**, no. 11, 115006 (2019) [arXiv:1907.08109 [hep-ph]].
 - [51] S. Gardner and X. Yan, arXiv:1907.12571 [hep-ph].
 - [52] M. Badziak and K. Sakurai, JHEP **1910**, 024 (2019) [arXiv:1908.03607 [hep-ph]].
 - [53] A. E. Cárcamo Hernández, S. F. King, H. Lee and S. J. Rowley, arXiv:1910.10734 [hep-ph].
 - [54] G. Hiller, C. Hormigos-Feliu, D. F. Litim and T. Steudtner, arXiv:1910.14062 [hep-ph].
 - [55] N. Haba, Y. Shimizu and T. Yamada, arXiv:2002.10230 [hep-ph].
 - [56] I. Bigaran and R. R. Volkas, arXiv:2002.12544 [hep-ph].
 - [57] S. Jana, V. P. K. and S. Saad, arXiv:2003.03386 [hep-ph].
 - [58] L. Calibbi, M. L. López-Ibáñez, A. Melis and O. Vives, arXiv:2003.06633 [hep-ph].
 - [59] R. Harnik, J. Kopp and P. A. N. Machado, JCAP **1207**, 026 (2012) [arXiv:1202.6073 [hep-ph]].
 - [60] W. Altmannshofer, S. Gori, M. Pospelov and I. Yavin, Phys. Rev. Lett. **113**, 091801 (2014) [arXiv:1406.2332 [hep-ph]].
 - [61] W. Altmannshofer, S. Gori, J. Martín-Albo, A. Sousa and M. Wallbank, Phys. Rev. D **100**, no. 11, 115029 (2019) [arXiv:1902.06765 [hep-ph]].
 - [62] X. G. He, G. C. Joshi, H. Lew and R. R. Volkas, Phys. Rev. D **43**, 22 (1991).
 - [63] F. Jegerlehner and A. Nyffeler, Phys. Rept. **477**, 1 (2009) [arXiv:0902.3360 [hep-ph]].
 - [64] M. Lindner, M. Platscher and F. S. Queiroz, Phys. Rept. **731**, 1 (2018) [arXiv:1610.06587 [hep-ph]].
 - [65] P. F. de Salas, D. V. Forero, C. A. Ternes, M. Tortola and J. W. F. Valle, Phys. Lett. B **782**, 633 (2018) [arXiv:1708.01186 [hep-ph]].
 - [66] A. M. Sirunyan *et al.* [CMS Collaboration], Phys. Rev. D **100**, no. 5, 052003 (2019) [arXiv:1905.10853 [hep-ex]].
 - [67] G. Aad *et al.* [ATLAS Collaboration], JHEP **1509**, 108 (2015) [arXiv:1506.01291 [hep-ex]].